

Thermal-Shock Resistant Cement for Heat Storage

Tatiana Pyatina and Toshifumi Sugama

Brookhaven National Laboratory

Keywords

Energy storage, geothermal, cement, calcium-aluminate cement, thermal shock, fly ash, TSRC

ABSTRACT

Geothermal energy may offer both daily and seasonal stabilization of grid operations using Reservoir Thermal Energy Storage (RTES) systems alone or in combination with solar energy. Long-term reliable performance of such systems will depend on the wellbore integrity. One of the main stresses compromising well performance is related to the frequent and possibly significant temperature variations caused by injections of very hot or cold fluids. The cycles may be of short (daily) or longer (seasonal) frequencies. During the frequent thermal cycling the cement sheath repeatedly undergoes thermal stresses by thermal expansion (microcrack development in sheath by compressive stress) and cool contraction of casing (micro-annulus development between the sheath and casing by tensile stress).

This work focused on repeated stress conditions, subjecting cement sheath and bulk cement to multiple stress cycles, while monitoring dimensional stability of cement, cement's coefficient of thermal expansion (CTE), changes in mechanical properties and phase transitions to define physicochemical factors governing stability and degradation of cement. Advanced calcium-aluminate-alkali activated fly ash, F (FAF), Thermal Shock Resistant Cement (TSRC) was tested while OPC modified with silica flour served as a reference. OPC-based cement sheath broke in the first cycle forming wide continuous cracks, losing 84% of the bond strength and compromising carbon steel (CS) corrosion protection so that severe corrosion of CS was observed after 20 TS cycles (250°C dry→18°C hydrothermal). TSRC performed significantly better under these conditions losing 11% of the bond strength and for the most part providing CS corrosion protection. The phase transition analyses showed importance of formation of amorphous aluminum-rich interfacial layer for good bond durability and corrosion protection. Future efforts for optimized RTES and energy generation are proposed.

1. Introduction

To insure robust grid performance so that energy would be delivered whenever requested, energy storage can help to compensate for fluctuations in energy production. Geothermal reservoirs are an obvious attractive solution for energy storage and production on request. However, for a robust long-term performance of a geothermal reservoir as a storage, it must withstand repeated

thermal stresses during the injection, storage and production of heated steam. The higher the temperature of the stored steam the more economical is the heat recovery. In case of the solar energy production the steam temperatures may exceed 300°C imposing significant stresses on the storage reservoir.

The aim of this project is to facilitate combining energy production (solar, wind) and energy storage to smooth out fluctuations in energy production caused by changing weather and time of day, reduce demand charges and provide clean energy to the grid when it is most valuable, through the reliable use of geothermal reservoir by developing and testing innovative cementitious materials that provide economical and resilient natural energy storage under conditions of repeated thermal stresses and elevated temperatures. In well construction, integrity of the cement is essential to provide zonal isolation, prevent casing corrosion and support the well structure. Cement sheath failure to fulfill any of its tasks may result in catastrophic events where the well would be abandoned and a new well would have to be constructed. There are numerous examples of such well failures, including oil and gas well failure in the Gulf of Mexico (compromised zonal isolation) and an ultra-high temperature geothermal well failure in Iceland (extensive casing corrosion). The geothermal wells are especially difficult for cements to survive because of the harsh environments and significant thermal and mechanical stresses (Berra et al., 1988; C. Teodoriu, Kosinowski, Amani, Schubert, & Shadravan, 2013). The known solutions for oil and gas wells most of the time are not applicable for geothermal cements because of the high temperatures (Catalin Teodoriu & Falcone, 2009). Organic additives commonly used to modify cement properties for improved performance cannot survive under these conditions; they decompose releasing CO₂ and compromising cement and well integrity. The stresses are even higher for wells used for heat storage and subjected to repeated hot steam injections. Another issue in adopting oil field cement solutions is expected life span of a well, which is generally much shorter for oil and gas recovery than for the heat recovery and storage. That situation requires targeted solutions for cement composites that would provide durable, economical zonal isolation and well integrity under the conditions of repeated thermal stresses.

For the last six months a joint BNL-SNL team worked on enhanced Thermal Shock-Resistant Cement (TSRC) (Sugama & Pyatina, 2019) to facilitate its use during severe and moderate repeated thermal cycling in geothermal and/or oil and gas wells to mitigate microcrack and microannulus development under the conditions expected in energy storage wells. The team used a common Portland cement modified with silica flour for high-temperature applications as a baseline. Particular attention was paid to the cement-casing interfacial bond that often is the weakest point of cement zonal isolation (Pyatina, Sugama, & Zaliznyak, 2017). This paper presents the results of this work, the main conclusions drawn from it, and necessary future efforts.

2. Experimental

Three types of thermal cycling tests were performed with two cement formulations (Figure 1): 1) TSRC and 2) OPC, class G, modified with 30% by weight of blend silica flour, tested as a high-temperature reference cement in severe 250°C → 18°C cycles. (Only TSRC was tested in moderate hydrothermal cycles (100°C → 18°C).) The TS conditions were reproduced in two types of experimental set ups: severe and moderate. Under the severe TS the bulk and sheath

cement samples were subjected to repeated 250°C autoclaving followed by 4 hrs at 250°C dry heat and 15 min 18°C cold water exposure directly after the heat either by cold water passing through the tubes (100 ml/s) of the sheath samples or bulk cement samples placed into a beaker with cold water. Although the dry conditions could be expected only in hot rock formations, this set up reproduces both compressive stress (during the heat) and tensile stress (during the cold water going through the casing tube) of cement and is relevant for the combined solar-geothermal heat recovery-storage where very high temperatures are reached during solar heating. Furthermore, the heat conditions expose cement to carbon dioxide commonly present in geothermal wells and causing cement carbonation, which is similar under dry heat and hydrothermal conditions. Finally, the advantage of severe conditions is acceleration of cement damage allowing identification of critical parameters for its stability and degradation in relatively short time.

Additionally, the severe conditions were modeled by two types of initial heat exposure after the 24hrs of hydrothermal curing at 250°C. In the first set up the temperature was ramped up to 250°C (10°C/min temperature increase rate) and the samples stayed at that temperature overnight before TS cycles. In the second set up the samples were initially heated to 60°C for 2 days and then exposed to 250°C (5°C/min temperature increase rate) for 4 hrs in each cycle before cold water exposure. Fast temperature increase causes cement shrinkage and damage of the cement-metal bond. This allows for accelerated testing of the potential damage. On the other hand, such conditions are not likely in geothermal wells where temperature increase is usually very gradual and may happen over several days after the cement placement. The second set up used in the testing modeled slower heating of cement samples with lower shrinkage.

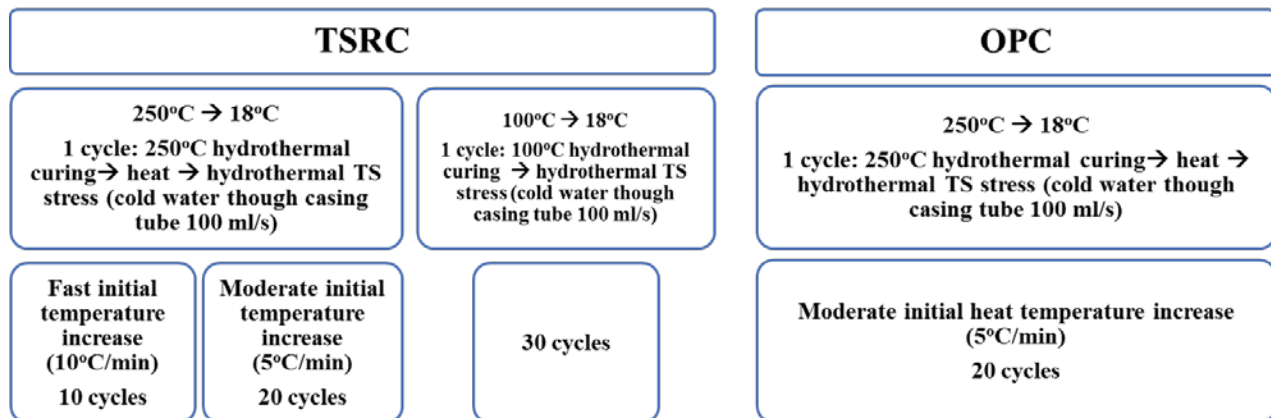


Figure 1: Summary of TS cycle experiments conducted with TSRC and OPC/SiO₂ formulations

The data analyses for the control samples after the exposure of fast- and slow-heated samples showed that after the cycling there was no significant difference in phase compositions and morphologies of TSRC samples prepared with two different initial heating schedules, however, the mechanical properties of the samples differed significantly.

Cement formulations, compositions and suppliers of the starting materials can be found elsewhere (T Sugama & Pyatina, 2019). Micro carbon fibers (MCF) were used at 6% by weight of blend in both formulations to improve the compressive toughness, and control the cracks width and propagation as described in (Sugama & Pyatina, 2019), (Pyatina & Sugama, 2014). Dyckerhoff, type North, oil field, class G cement was used to prepare OPC/SiO₂ blend.

Calculations of CTE assumed that hydrating cement is a new material after each cycle because of the on-going composition changes. The measured values of the cement bar length were compared against its cold length value at each cycle and not to its original length. For the moderate thermal shock, the temperature difference for the coefficient calculations was taken as 72 °C and not 82 °C accounting for some cooling of the bar during the measurements. For the severe thermal shock, the temperature difference was taken to be 220 °C for the same reason. The number of cycles over which coefficients were averaged was decided based on the similarity of the values: averaging was done over 5 cycles for similar values; for the first outstanding values in the cases of TSRC and OPC/SiO₂ heated to 250 °C the averaging was done starting with the second cycle. Because of the outstanding first CTE value it was concluded that the materials underwent major changes after the first cycle and then the changes were more gradual.

3. Results and discussion

3.1 TSRC-moderate TS

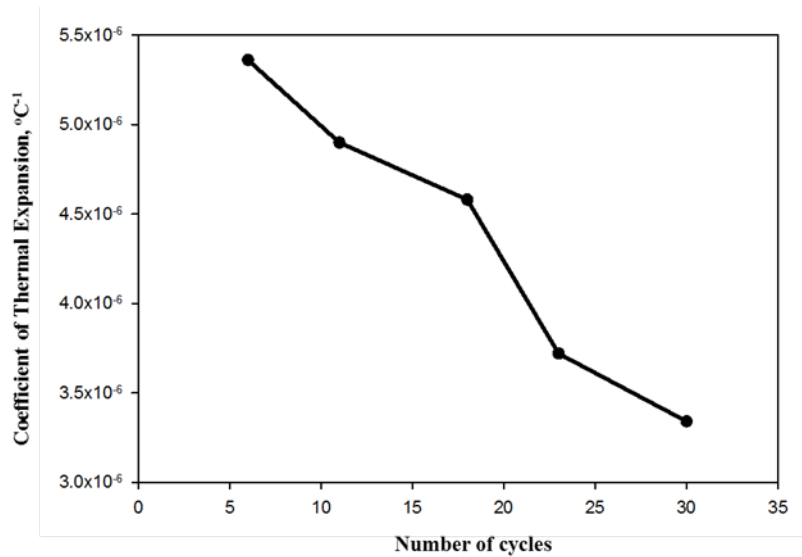
3.1.1 Mechanical properties and CTE

TSRC samples' mechanical properties before and after 12 and 30 moderate hydrothermal TS cycles are given in Table 1. Compressive strength, sheath shear bond strength, and Young's modulus increased consecutively during the moderate hydrothermal cycling. The compressive strength increased by 134%, the bond strength by 150% and the Young's modulus by 45%. These data indicate that the moderate hydrothermal TS cycling does not compromise cement hydration, alkali reactions and phase transitions responsible for development of mechanical properties. The increase in the bond strength to more than 20% of the compressive strength is remarkable and shows excellent material's affinity to the CS. Increase in the Young's modulus corresponds to decreased material's elasticity or increased rigidity as it ages and builds up the strength. This stiffness of the material may increase because of increased sample's nano- or micro-crystallinity or further hydration and reactions of the non-reacted materials in the sample with densification of the amorphous hydrates and reaction products. The result of such changes is necessarily reflected in changed thermal behavior of the material in response to the thermal stresses. Figure 2 shows changes in CTE with increased number of moderate thermal cycles.

Table 1: Mechanical properties of bulk and sheath TSRC cement samples before and after moderate hydrothermal TS cycles.

Number of cycles	Compressive strength, psi	Young's modulus, psi	Sheath-shear bond strength, psi
0	700 ± 125	128680 ± 59330	140 ± 40
12	1450 ± 270	136970 ± 22080	260 ± 60
30	1640 ± 90	187245 ± 8940	350 ± 40

CTE was measured after each cycle and averaged over each 5-6 cycles resulting in 5 average points over the 30 cycles.

**Figure 2: Coefficient of thermal expansion (CTE) for TSRC as a function of the number of moderate hydrothermal TS cycles.**

There is a clear trend in CTE changes during the cycling: CTE slowly decreased over 30 thermal cycles by nearly 40% from $5.4 \times 10^{-6} \text{ }^{\circ}\text{C}^{-1}$ (first 6 cycles) to $3.3 \times 10^{-6} \text{ }^{\circ}\text{C}^{-1}$ (last 6 cycles). (The coefficient of thermal contraction (not shown) increased respectively from $(-6.8 \times 10^{-6}) \text{ }^{\circ}\text{C}^{-1}$ (first 6 cycles) to $(-3.8 \times 10^{-6}) \text{ }^{\circ}\text{C}^{-1}$ (last 6 cycles)). The reason for the change is likely continuous slow cement hydration and alkali reactions of FAF under the test conditions resulting in more rigid, dense structure with lower CTE, which is also reflected by increased Young's modulus of the material.

Since the CTE of steel does not change in the thermal cycling this change in cement CTE leads to increased difference between the two materials in their expansion and contraction and

increased risk of the interfacial bond damage during continuous use under conditions of moderate thermal stress.

In summary, thirty moderate TS cycles did not compromise mechanical properties of the TSRC sheath on CS, both matrix compressive strength and interfacial bond strength increased during the continuous curing and the cycling. XRD, FTIR analyses (not shown) suggested that the crystallization of the cement was slow at this temperature and mostly amorphous hydrates and reaction products formed both in the matrix and at the interface. The fact that amorphous interface product formed strong bond that increased at longer curing times suggests that amorphous interfacial phase may be favorable for the durable composite-metal bond. FAF particles reacted only partially suggesting remaining self-healing capacity of the cement at longer curing times in the case of the damage (Sugama & Pyatina, 2019). However, one concern was continuous decrease in CTE of the cement resulting in increasing difference between CTE of the cement and CS and higher risk of the interfacial bond damage after longer cycling.

3.2 TSRC and OPC/SiO₂ composites– severe dry TS

3.2.1 Samples' appearance

Figures 3 and 4 show changes in the appearances of the reference cement OPC/SiO₂ and TSRC sheath samples after the severe cycling. The passage of the water through the casing with OPC/SiO₂ sheath was accompanied by a bursting sound and wide cracks formed in the composite sheath during the first cycle. The cracks were going through the whole length of the composite sheath and widened in 20 cycles. The color of the samples changed from grey to red because of the corrosion of the CS tubes under the cement sheath. This clearly indicated that cement did not protect the casing anymore.

TSRC, on the other hand, survived 9 cycles before thin, hair cracks formed in the 10th cooling cycle. The cracks formed on the edges of the samples and did not continue through the entire samples' length. These cracks propagated further along cement sheaths in 20 cycles. The color of the cement did not change except for some red spots at the top and bottom of the samples where CS tubes were open to the curing environment.

The final appearance of the samples and the interface between the tested cement composites and the CS tubes are shown in Figure 4. The difference in colors of the outside sheath layer reflects the conditions of the interface for OPC/SiO₂ and TSRC samples. The metal under the OPC/SiO₂ sheath corroded completely forming corrosion scale that detached from the tube with the cement sheath coloring the sheath itself. There was no cement attached to the tube. In the case of TSRC the casing was partially covered with the protective cement layer and corrosion spots appeared only in some locations.

There were no cracks in bulk samples of TSRC or OPC/SiO₂ composites after 20 severe TS cycles.

The result was similar (not shown) for TSRC samples heated directly to 250°C after the initial curing (fast temperature increase rate) – the thin crack formed at the edges of the cement sheath after the first 10 cycles of TS; however, corrosion spots were not detected at the interface after the first 10 cycles.

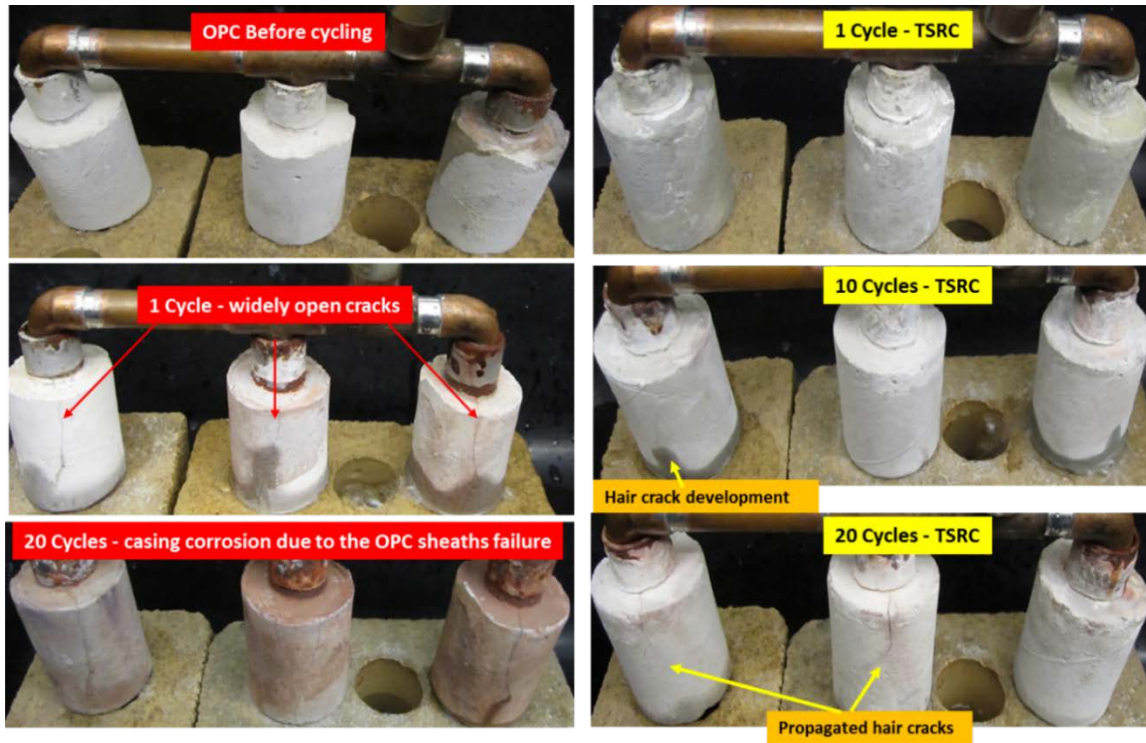


Figure 3. Changes in the appearance of OPC/SiO₂ (left) and TSRC (right) sheath samples during the severe cycling (one cycle: 250°C dry heat → cold water through the casing → 250°C hydrothermal curing).



Figure 4. Appearance of OPC/SiO₂ sheath samples (top) and TSRC sheath samples (bottom) after 20 severe TS cycles

3.2.2 Mechanical properties

Tables 2 and 3 give results of the mechanical properties measurements for the TSRC samples before and after 10 TS cycles (fast rate of temperature increase) or 20 TS cycles (moderate rate of temperature increase). In both cases the compressive strength of the samples did not change significantly while the bond strength decreased. Interestingly, the Young's modulus did not increase with the continuous cement curing and cycling. This is a positive feature since cements with lower Young's modulus are less susceptible to failure under common mechanical stresses during well operations. The most significant difference for the two tested initial rates of temperature increase was significantly lower sheath-shear bond strength and higher strength loss during the TS cycling for the system cured under the fast rate of initial temperature increase. The bond strength was nearly half of that for the system cured under moderate rate of temperature increase and the bond loss was >30% in 10 cycles compared to 11% loss in 20 cycles for the TSRC samples subjected to the moderate initial temperature increase rate. As was mentioned earlier the heating of the well is unlikely to go as fast as tested in these experiments; nevertheless this parameter may have to be taken into consideration during well operations – slow well-temperature increase and allowing an additional time before the start of the operations may significantly help preserving the well integrity.

Table 2. Mechanical properties of 250°C → 18°C thermal shock cycle test results for TSRC for moderate rate of the initial temperature increase

Number of cycles	Compressive strength, psi	Young's modulus, psi	Sheath-shear bond strength, psi
0	2030 ± 90	200110 ± 26810	180 ± 6
20	2085 ± 170	190990 ± 59820	160 ± 10

Table 3. Mechanical properties of 250°C → 18°C thermal shock cycle test results for TSRC for fast rate of the initial temperature increase

Number of cycles	Compressive strength, psi	Young's modulus, psi	Sheath-shear bond strength, psi
0	2040 ± 120	217270 ± 11270	95 ± 6
10	1950 ± 110	18125 ± 1960	65 ± 11

Table 4 shows results of the mechanical tests for OPC/SiO₂ blend. The initial compressive strength of this blend was more than double that of TSRC while the bond strength was similar (for the similar moderate rate of the initial temperature increase). (This unusually high bond strength for the OPC/SiO₂ blend is due to the presence of MCF in the formulation.) Hydration of this composite was faster resulting in faster strength build up and higher Young's modulus indicative of a more brittle material (Toshifumi Sugama & Pyatina, 2019). Both compressive strength and modulus did not change much during the cycling; however, the bond strength decreased dramatically by 84%. These data agree with the visual observations of crack formation in OPC/SiO₂ sheath samples and strong samples corrosion because of the poor protection of the carbon steel by the de-bonded cement sheath.

Table 4. Mechanical properties of 250°C → 18°C thermal shock cycle test results for OPC/SiO₂ for moderate rate of the initial temperature increase

Number of cycles	Compressive strength, psi	Young's modulus, psi	Sheath-shear bond strength, psi
0	2040 ± 120	217270 ± 11270	95 ± 6
10	1950 ± 110	18125 ± 1960	65 ± 11

3.2.3 Dimensional changes

Figure 5 shows changes in dimensions of TSRC and OPC/SiO₂ samples during the severe cycling. The behavior of the two composites is different – TSRC sample expands and OPC/SiO₂ sample does not change significantly its dimensions during the cycles. The expansion is due to the formation of new phases, phase transitions and, possibly, carbonation of the sample during the heat exposure. Slow FAF reactions may contribute to gradual phase changes and formation of new phases leading to the sample expansion over the test period. The changes in OPC happen over a short time-period with faster crystallization of hydrates and reactions with silica. Carbonation of the OPC/SiO₂ sample during the heating did not seem to change its dimensions.

Shrinkage is one of the reasons of poor cement-casing bonding, so the slightly expansive nature that TSRC demonstrated in the cycling tests is favorable for the interfacial bonding in agreement with the mechanical tests that showed bond failure for OPC/SiO₂ sheath samples while relatively small bond strength decline for TSRC sheath samples.

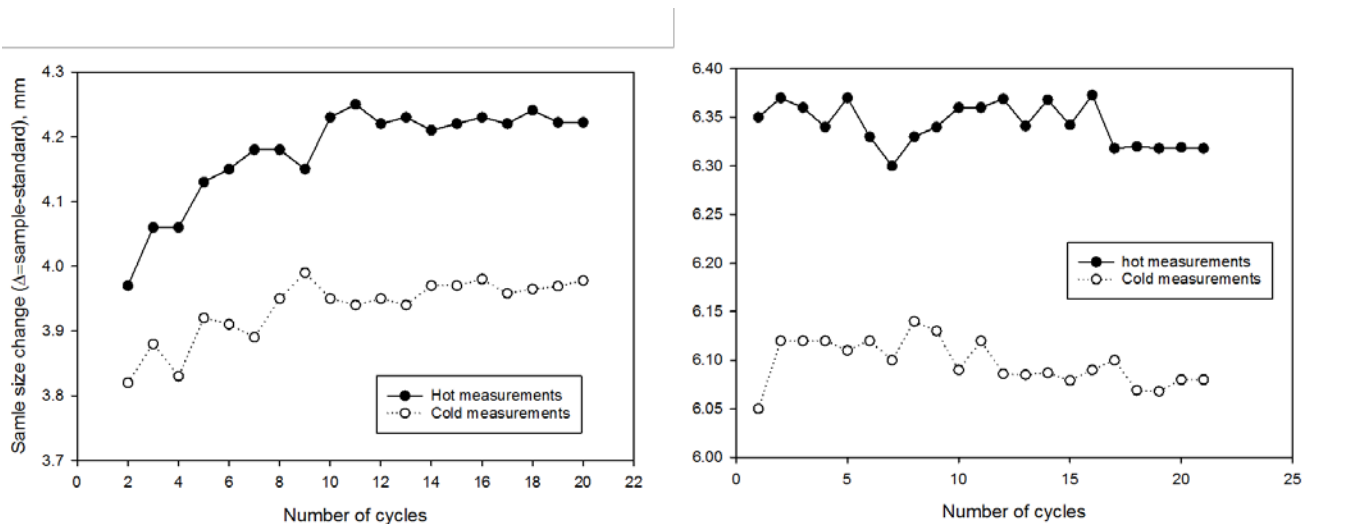


Figure 5. Sample size changes (difference between the standard bar and the cement sample) over the cycling period for TSRC (left) and OPC (right) exposed to severe TS cycling: 250°C dry heat → 18°C water.

3.2.4 Coefficients of thermal expansion (CTE)

The changes in CTE in severely stressed cements were similar for both TSRC and OPC/SiO₂ samples: the CTE dropped in the first cycles and then stabilized, the further changes were moderate especially in the case of the OPC-based formulation (Figure 6). For TSRC the coefficient slightly increased during the 20 severe cycles after the initial drop. The fast change in the CTE of TSRC during the severe cycling was quite different from the gradual CTE decrease of the composite exposed to the moderate hydrothermal shock. By the end of the 20 cycles the CTE was ~20% lower than the control one. For the OPC-based formulation the CTE was ~17% below the CTE of the control sample.

For comparison the CTE of steel remained constant during the cycling while the CTE of both composites decreased (Figure 6) increasing the difference with the CTE of CS. However, the change was not dramatic and cannot account for the significant difference in the bond strength changes of the two tested composites. CTE changes at longer testing times could be more significant further affecting the bond strength.

In summary, the CTE change in the first cycle was the most significant in the severely cycled dry-heated composites. Further changes were minor. Such a decrease in the CTE occurred while the composite was still reacting with formation of new cementitious phases both in the matrix and at the interface and accompanied changes in mechanical properties. Continuous composite reactions however, did not further decrease the CTE but stabilized it at the experimental conditions. TSRC and OPC-based composites had similar trends of CTEs changes over the test period, so these changes cannot account for the dramatic difference in the bond strength and corrosion protection behavior of these composites.

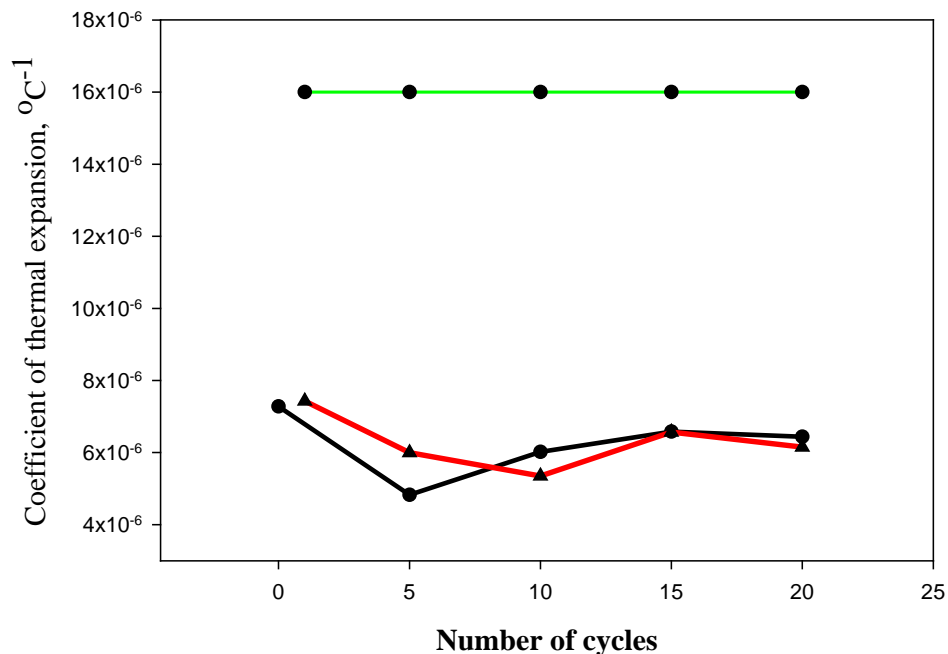


Figure 6. Changes in CTE of CS (green), TSRC (black) and OPC (red) exposed to severe TS cycling: 250°C dry heat → 18°C water.

3.2.5 Crystalline composition (XRD) - TSRC

Figure 7 shows XRD patterns of TSRC samples before (red) and after (blue) 20 severe dry heat TS cycles. For the matrix the major changes that occurred during the cycling included 1) disappearance or decrease in the intensities of the starting materials (e.g. sillimanite from FAF (ICDD: 04-007-8854), 2) low-silicon phases such as luicite (ICDD: 01-076-8733/00-038-1423) and sodalite (ICDD: 01-070-5028) were replaced by calcium-aluminum silicate dmisteinbergite (ICDD: 04-011-5220) that becomes the major crystalline reaction phase along with crystallization of silica (ICDD: 01-077-8639), 3) there was increased sample carbonation, with formation of cancrinite group silicon-rich mineral cancrisilite (ICDD: 04-020-1220) and clearly increased peak of calcite (ICDD: 04-002-9082).

For the interface there was a couple of striking changes after the cycling in addition to the disappearance of the FAF peaks: 1) zeolite, analcime, detected in the interface control sample after the cycling was replaced by the carbonated cancrinite group mineral cancrisilite (ICDD: 04-020-1220); 2) feldspar mineral predominant in the matrix was also detected at the interface, dmisteinbergite (ICDD: 04-011-5220), 3) the calcite peak was even stronger at the interface than in the matrix.

In summary, the cycling resulted in further reactions of FAF with release of additional silicon that assisted in formation of silicon-rich phases both at the interface and in the matrix and carbonation of the composite with formation of desirable dense cancrinite group mineral phase (cancrisilite) and undesirable calcite phase, especially at the interface, where its large crystals negatively affect the bond strength.

3.2.6 Amorphous and crystalline compositions (FTIR) – TSRC

Figure 8 shows FTIR spectra of TSRC samples before and after 10 or 20 severe dry heat cycles. Comparison of the spectra clearly shows increased crystallinity of the samples during the cycling: the ratio of absorbance peaks between crystalline and amorphous calcium/sodium-aluminum-silicate ($898\text{cm}^{-1}/994\text{cm}^{-1}$) increases unambiguously. Compared to the control the ratio increases by 2.4 times for the matrix and by more than 9 times for the interface. Such increase of the interface crystallinity increases vulnerability of the composite-metal bond. In agreement with the XRD results there is an increase in carbonated hydrates (1514 and 1403cm^{-1}), silica (11.76cm^{-1}) and crystalline aluminum-silicate hydrates (675cm^{-1}). There is also a clear increase in silica gel both at the interface and in the matrix due to the further decomposition of FAF. This phase is a source of silicon for further crystallization of silica and silicon-rich phases detected by XRD. The interface has growing amount of aluminum oxide hydroxide, which agrees with the XRD findings of the TSRC samples after 10-cycles (not shown).

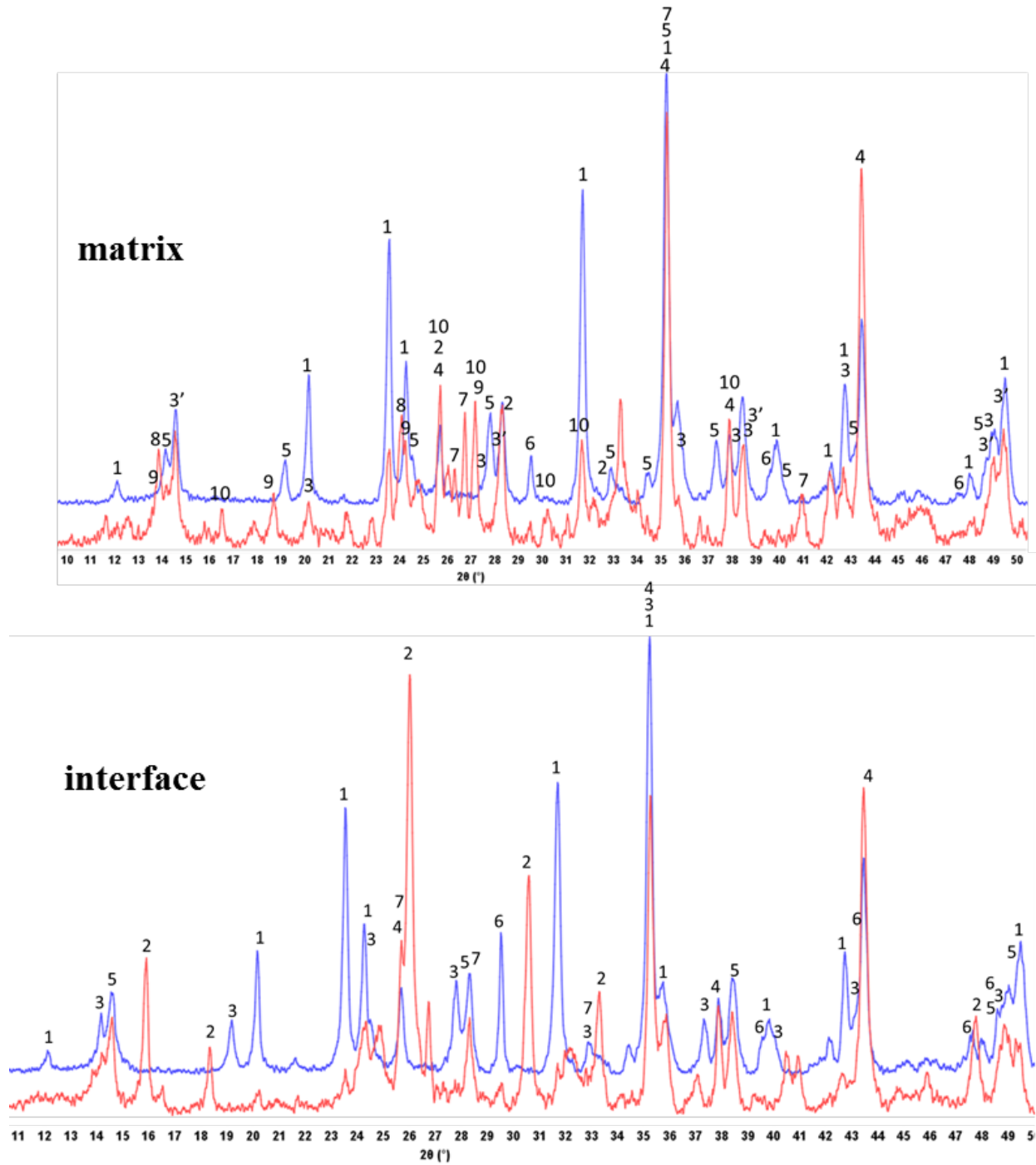


Figure 7. XRD patterns of matrix and interface of TSRC before (red) and after (blue) 20 severe dry heat → cold water TS cycles.

Matrix: 1-dmisteinbergite, 2-silica, 3-tohdite, 4-corundum, 5-cacrisilite, 6-calcite, 7-sillimanite, 8-sodalite, 9-hydroxycancrinite, 10-luicite

Interface: 1-dmisteinbergite, 2-analcime, 3-cancrisilite, 4-corundum, 5-boehmite, 6-calcite, 7-silica

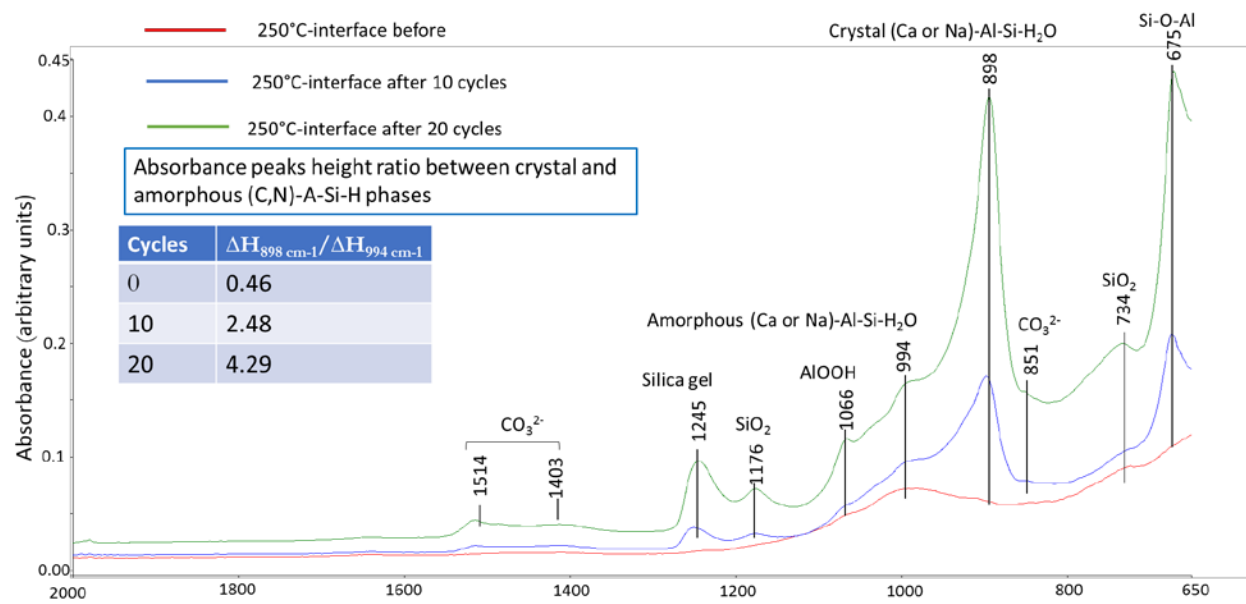
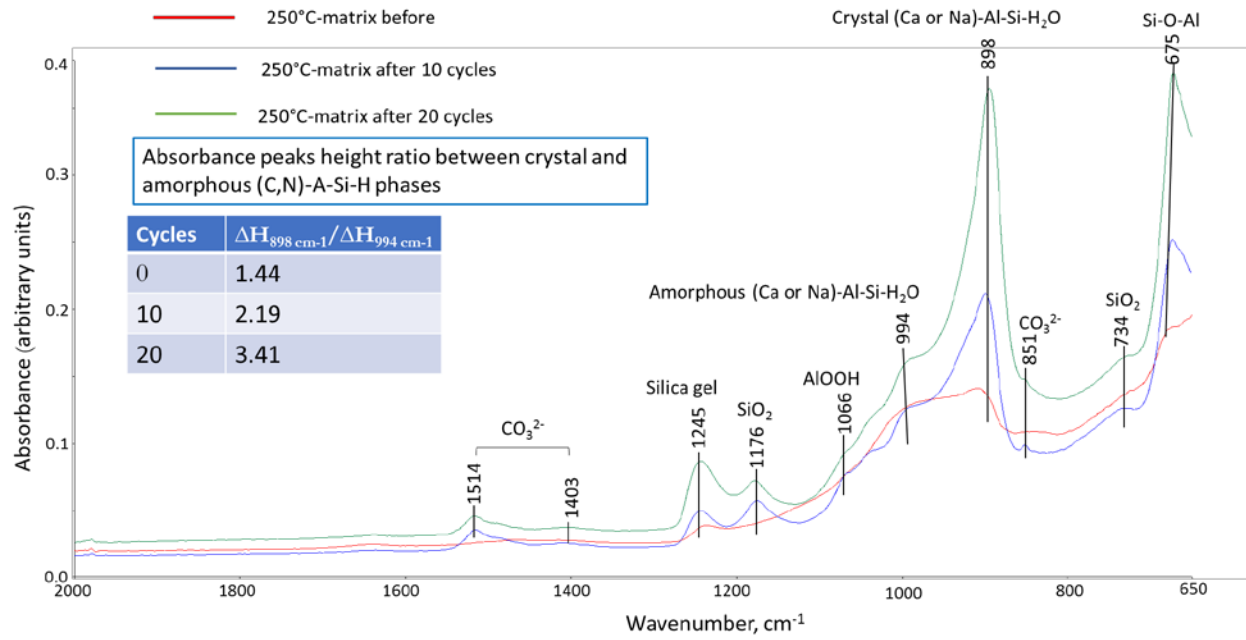


Figure 8. FTIR spectra of TSRC matrix and interface samples before and after the severe TS cycles.

3.2.7 Morphology and elemental analyses (SEM/EDX) – TSRC

Figures 9 and 10 show typical TSRC matrix and interface microstructures and their elemental compositions. (Note that the silver signal visible on all the photomicrographs is from the silver coating used to eliminate charging effects during the measurements.) After 20 severe cycles TSRC matrix was for the most part amorphous (Figure 9). There were non- or partially-reacted FAF particles and carbon fibers imbedded into the matrix. The elemental composition of the matrix was aluminum-rich calcium-aluminum silicate hydrates. Small platelet-like structures formed among the amorphous matrix had elemental composition of dmisteinbergite identified by XRD. This hydrate presented dense features often seen in large circular arrangements in the matrix. Bigger crystals of $\sim 30 \mu\text{m}$ (Figure 10) had elemental composition of calcium carbonate.

Figure 10 shows two photomicrographs of the TSRC interface after 20 severe cycles. As for the matrix it was for the most part amorphous with some more defined features. The spots with no clear features were rich in aluminum. Those with some platelet-like structure had elemental composition of dmisteinbergite or cancrisilite. Iron was also measured in the platelets possibly because of the incorporation of the tetrahedral iron into the structure of the cancrisilite, reported earlier for cancrinite (Latham, Williams, & Duke, 1996). The two possible sources of iron are FAF and the CS. Since iron was detected at the interface but not in the matrix CS was its likely source. Such interactions could help improve interfacial bond strength. Carbon was difficult to identify unambiguously because of the carbon fibers distributed throughout the matrix. The layer next to the interface had better-visible features of separate platelets grown in different directions and tightly interconnected. The bigger crystals of 10-30 μm in size had elemental composition of calcium carbonate in agreement with both XRD and FTIR findings. These big crystals are unfavorable for the integrity of the interfacial layer and the bond strength.

In summary, morphological analyses showed for the most part amorphous structure at the interface rich in aluminum, similarly to the interface observed after 30 moderate cycles. Some interfacial phases with platelet-like appearance included iron from CS into their structures possibly improving the bonding. Presence of partially reacted FAF particles suggests that TSRC still has healing capacity after 20 severe TS cycles.

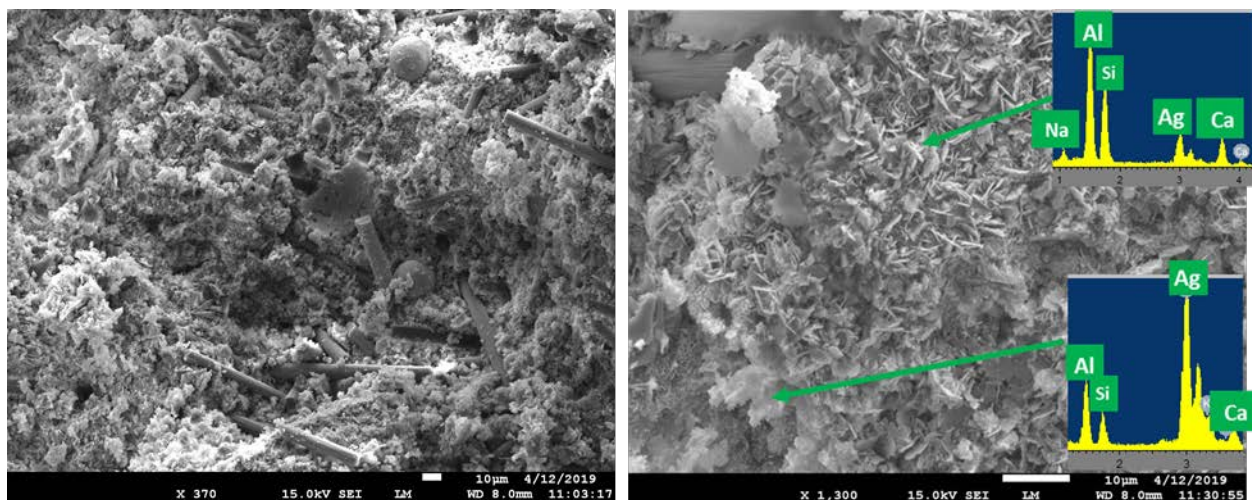


Figure 9: Scanning electron photomicrographs and elemental composition of typical TSRC matrix microstructures after 20 severe TS cycles.

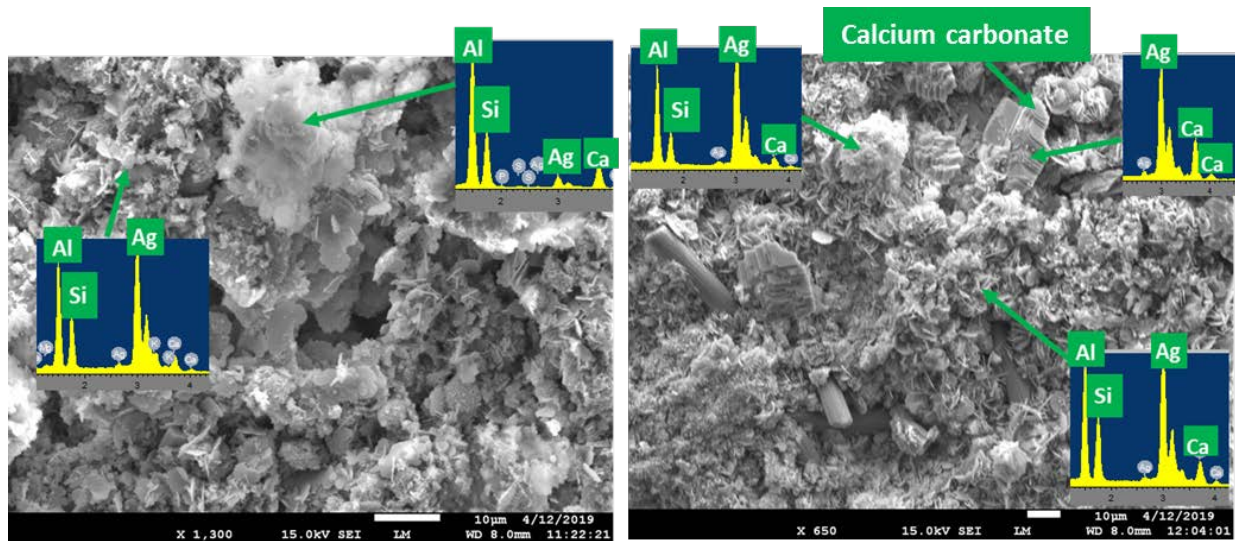


Figure 10: Scanning electron photomicrographs and elemental composition of typical TSRC interface microstructures after 20 severe TS cycles (left-metal side; right – cement side).

3.2.8 Crystalline composition (XRD) – OPC/SiO₂

Figure 11 shows XRD patterns of OPC/SiO₂ samples before (red) and after (blue) 20 severe dry heat TS cycles. Unlike for TSRC the matrix pattern of the treated samples was very similar to that of the control. The major crystalline phase was high-temperature calcium-silicate hydrate, xonotlite (ICDD: 00-023-0125). The major difference was appearance of the hydration products of the cement interstitial phase (C₄AF). The decrease in the shoulder at 2 θ ~12.42 is due to the hydration of this phase that forms such products as andradite (ICDD: 01-071-3855) and grossular hydroxylan (ICDD: 00-042-0570). There is also increase in the peak of calcium carbonate after the TS cycling.

For the interface the changes in the XRD patterns after the TS cycling were dramatic. The XRD pattern of the control interface sample was very similar to that of the matrix, dominated by xonotlite. After the cycling the xonotlite peaks disappeared; the new peaks matched hematite (ICDD:04-006-0285) and iron oxide hydroxide patterns (ICDD: 01-084-6030). Iron oxides gave the rust coloring to the interface. Since the casing was completely detached from the cement, the interface sample was scraped from the cement itself and some of the cement matrix hydrates contributed to the pattern (e.g. andradite and grossular present in the matrix). Additionally, iron and aluminum-containing phases formed at the interface, including calcium-aluminum-iron oxide (ICDD: 04-015-8014), srebrodolskite, aluminian (ICDD: 04-014-66-34) and grossular ferroan (ICDD: 01-082-9677). The patterns of the latter two phases strongly overlap with the first one and are not marked on the figure. There were also peaks of iron-calcium oxide, harmunite and calcium carbonate.

In summary, the crystalline composition of the OPC/SiO₂ is stabilized after the initial high-temperature curing with xonotlite being the predominant phase in the matrix. Only minor changes due to the further reactions of the calcium-iron-aluminate interstitial phase take place

during the cycling in the matrix. On the other hand, xonotlite is not stable at the interface – it decomposes, and casing corrosion and decomposition-cement-reaction products replace xonotlite. Iron from corroded metal forms new calcium-aluminum-silica-iron oxides. These products are unfavorable for the interfacial bonding. Noticeably, there are aluminum-containing reaction products predominantly present at the interface even for this formulation with low aluminum content.

3.2.9 Amorphous and crystalline compositions (FTIR) – OPC/SiO₂

Figure 12 shows FTIR spectra of OPC/SiO₂ samples before and after 20 severe dry heat cycles. The spectra of the matrix before and after the cycling resembled each other. The features of the spectrum after the cycling were not as well resolved as on the spectrum before it but all major peaks were present. The interface spectra before and after the cycling differed significantly in three major ways: 1) the major peak of calcium-silicate bonding at 968cm⁻¹ decreased drastically while there appeared the peak at 1005cm⁻¹ corresponding to the Fe-O-Si linkage in calcium-aluminum-iron-silica hydrates suggested by XRD analyses, 2) there was a noticeable increase in carbonate peaks at 1489 and 1453 cm⁻¹ and a peak at 877cm⁻¹ suggesting interface carbonation during the cycling and 3) increase in silica gel peak at 1200cm⁻¹. The decreased intensity of the peak of calcium-silicate hydrate, increased carbonate and silica gel peaks suggest decomposition of crystalline calcium silicates with formation of calcium carbonate and release of silica gel that partially crystallizes into quartz (peak at 669cm⁻¹). This carbonation process destroys cement at the interface and is of concern for geothermal environments that are generally CO₂-rich.

3.2.10 Morphologies and elemental analyses (SEM/EDX) – OPC/SiO₂

Figures 13 and 14 show typical OPC/SiO₂ matrix and interface microstructures and elemental compositions. After 20 severe cycles the composite matrix was dense with inclusion of holes (Figure 13). These holes were filled with small calcium-silicate crystals (~1 μM; Ca:Si = 4:5) and deposits of big calcium carbonate crystals. Crystals in the shape of long needles had typical elemental composition of xonotlite. Significant parts of the matrix were still amorphous and silicon-rich.

Figure 14 shows photomicrographs of OPC/SiO₂ interface with CS. The interface presented almost a powder-like crumbling amorphous product with granular-morphology for the most part, rich in silicon and iron in agreement with the FTIR findings of –Fe-O-Si- linkage. Some parts of the interface were fluffy-amorphous (top) and in addition to silicon and iron had aluminum and magnesium in their composition. Underneath this amorphous layer that was in contact with the CS there appeared tiny calcium-aluminate crystals. It is remarkable that for Ca-rich blend of OPC/SiO₂ there was no or little calcium in contact with the steel. Another remarkable feature was composite interactions with the carbon fibers: the fibers were covered with the silicon-iron amorphous composite hydrates that reacted with the fibers' surface. For comparison, the carbon fibers in the matrix were completely free of the cement – unlike iron-silicates, calcium-silicate hydrates did not interact with the carbon fibers. These observations suggest poor Ca interactions with CS and fiber surfaces.

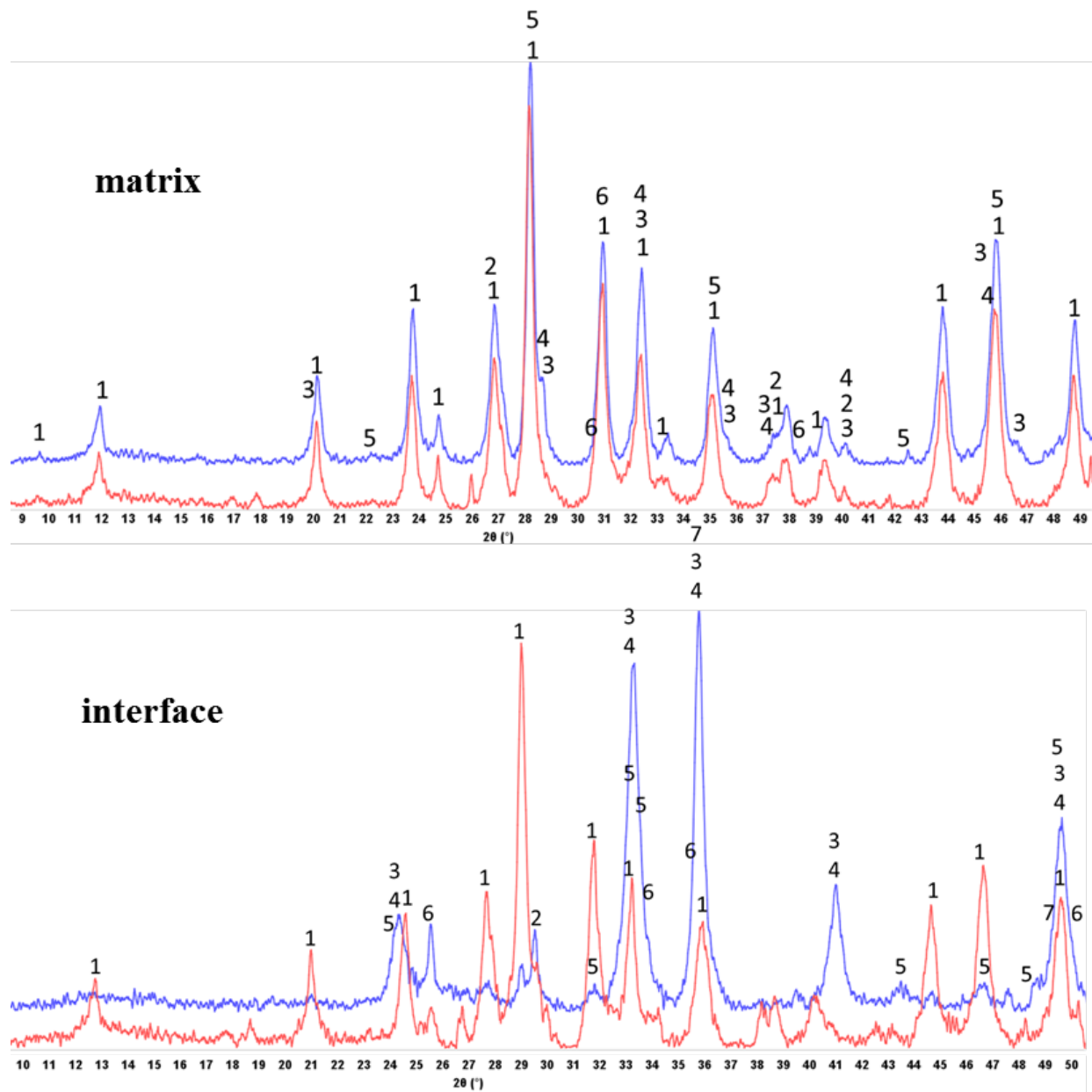


Figure 11. XRD patterns of matrix and interface of OPC/SiO₂ blend before (red) and after (blue) 20 severe dry heat → cold water TS cycles.

Matrix: 1-xonotlite, 2-silica, 3-andradite, 4-grossular hydroxylan, 5-calcium carbonate, 6-calcium hydroxide

Interface: 1-xonotlite, 2-silica, 3, 4- iron oxide hydroxide and hematite, 5-calcium-aluminum-iron oxides and hydroxides, 6-iron-calcium oxide (harmunite), 7-carbonate

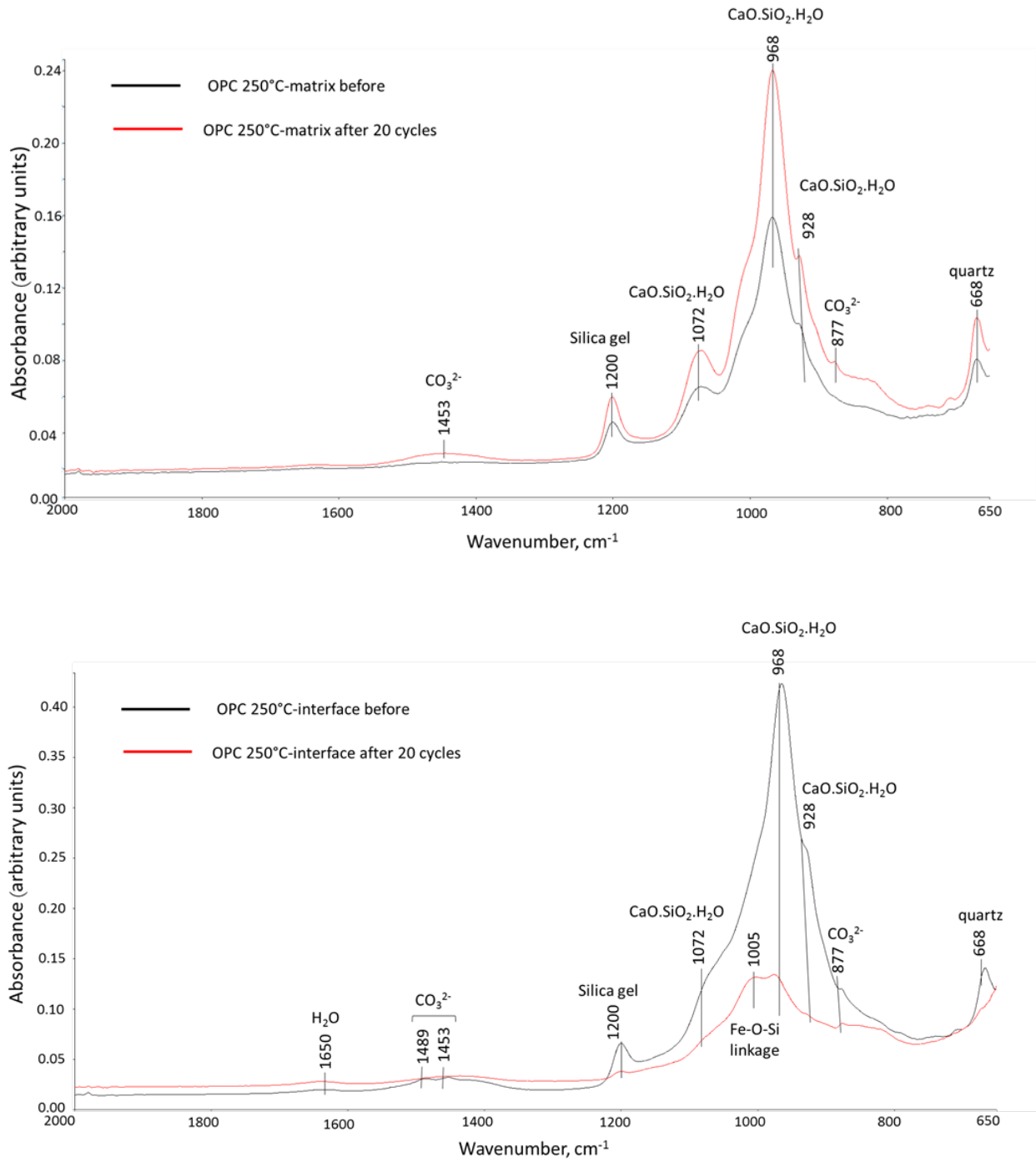


Figure 12. FTIR spectra of OPC/SiO₂ matrix and interface samples before and after 20 severe TS cycles.

3.2.11 Summary of microstructural studies

The microstructural studies demonstrated the following clear differences between TSRC and OPC/SiO₂ composites: 1) TSRC matrix underwent compositional changes during 20 severe TS cycles, these are mostly due to the slow reactions of FAF and carbonation with formation of high-temperature stable carbonated calcium-aluminum silicates. OPC/SiO₂ matrix composition did not change significantly in 20 severe cycles, calcium-silicates formed after the first day of high-temperature curing remained the major phases after the cycling. 2) The morphologies and compositions of TSRC matrix and interface were very similar. Composition of the OPC/SiO₂ composite interface drastically changed during the cycling – the originally formed hydrates were replaced by amorphous iron-aluminum-silicates disconnected from the matrix and metal surfaces, silica gel and calcium carbonates.

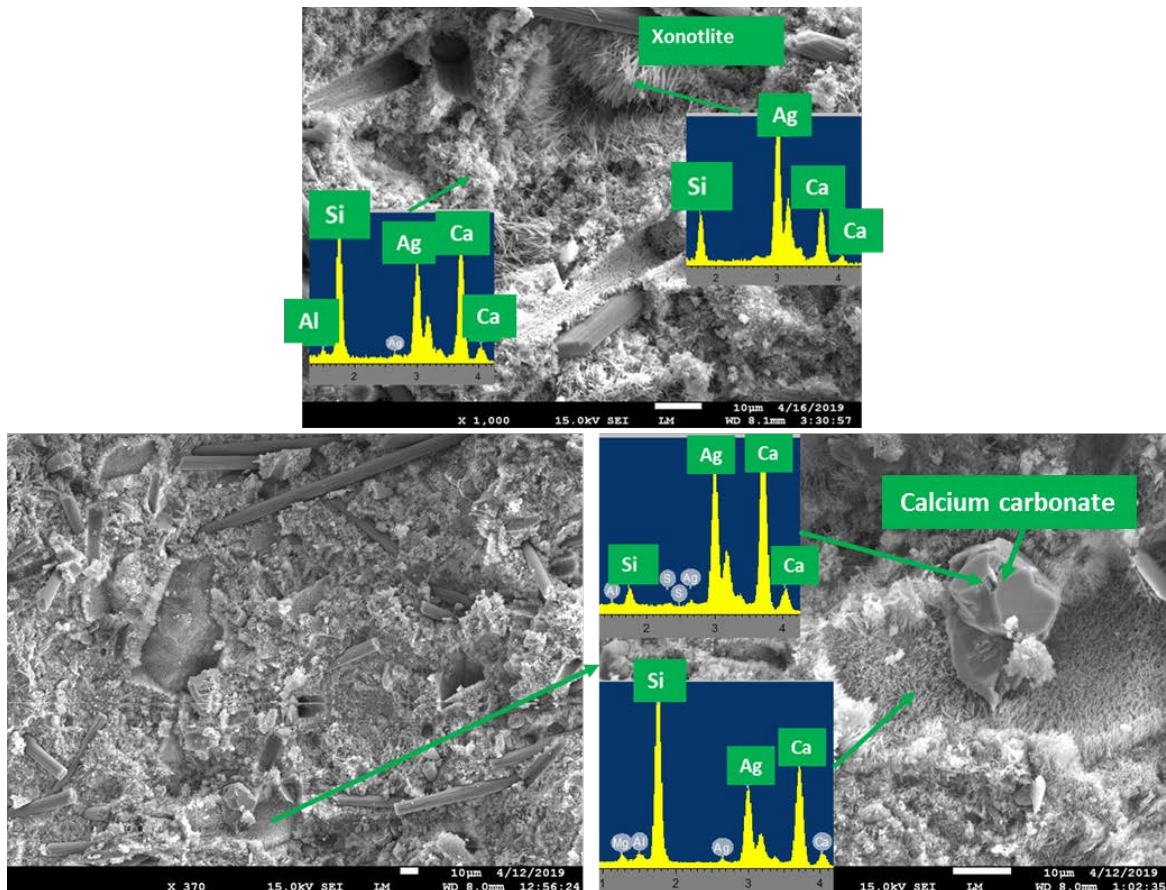


Figure 13: Scanning electron photomicrographs and elemental composition of typical OPC/SiO₂ matrix microstructures after 20 severe TS cycles.

The difference in the interfacial interactions of TSRC and OPC/SiO₂ composites could be explained by the differences in their chemistries. Highly alkaline slurries of both composites form protective layer at carbon steel casing, however the further interactions differ. In the case of TSRC readily available sodium metasilicate (Na⁺OSi(OH)₃⁻) reacts both with Al(OH)₄⁻ from calcium aluminate cement and with the metal surface protective layer (Fe-OH) to form NaOH and Fe-O-Si linkage further stabilized by the Al into iron substituted (Na)-silicon-aluminum-hydrates that later transfer to stable carbonates (cancrinite and cancrisilite). The EDX measurements suggested inclusion of iron into the cancrisilite/cancrinite network, possibility of which was reported earlier (Latham et al., 1996). Slowly reacting TSRC blend components, form predominantly amorphous phases at the interface, which can accommodate the new phases into the cement matrix. Below is schematics of possible formation pathways of interfacial TSRC phases.

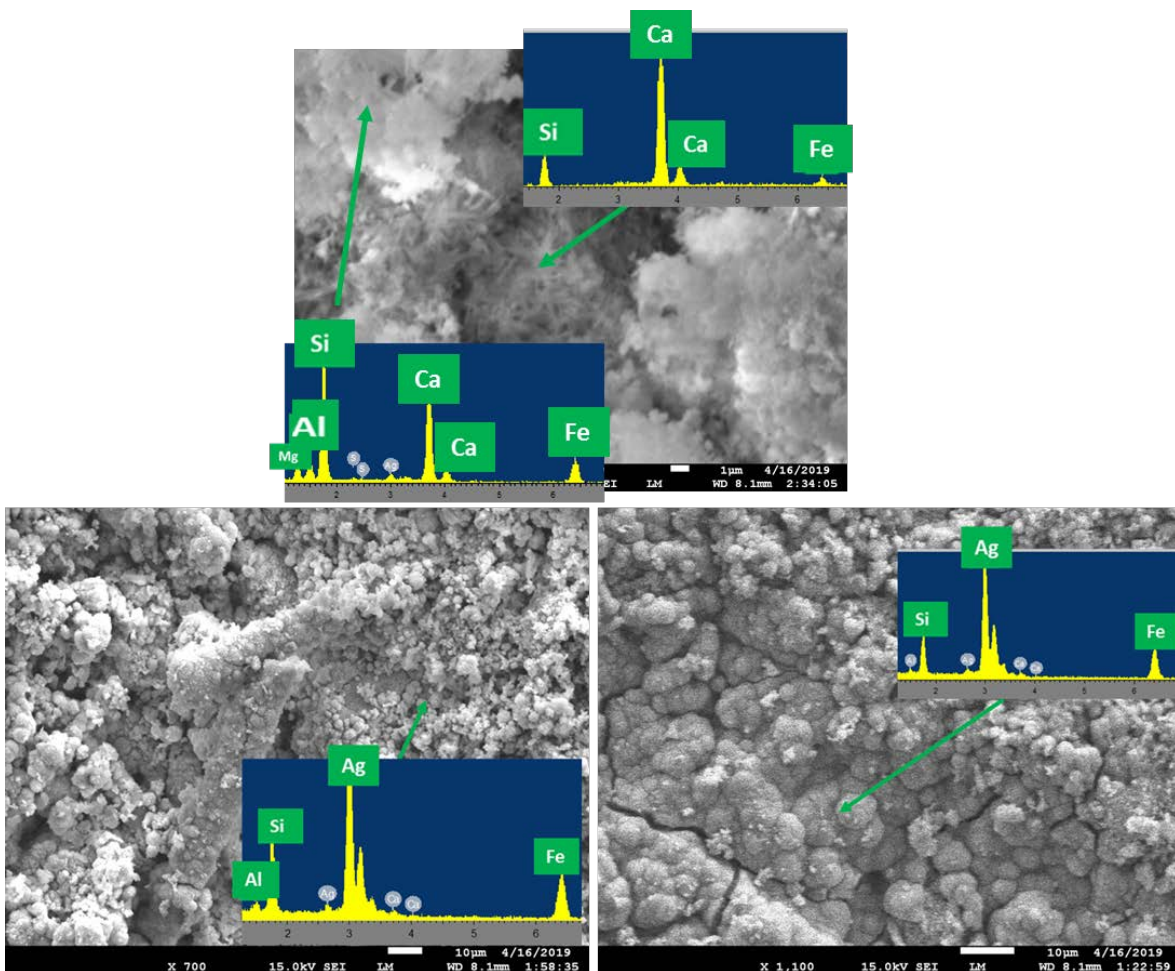
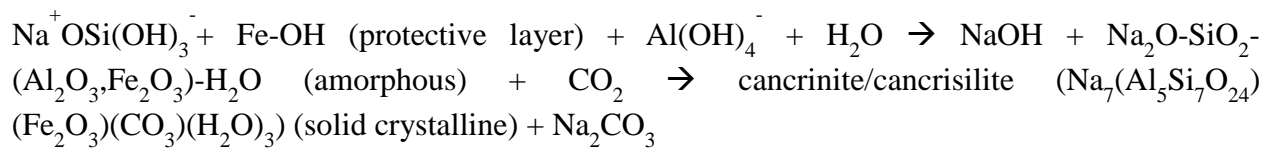


Figure 14: Scanning electron photomicrographs and elemental composition of typical OPC/SiO₂ interface microstructures after 20 severe TS cycles.

For the OPC/SiO₂ blend the Fe-OH also forms amorphous products with Fe-O-Si linkages at the interface. However, these are not included into a stable (Na)-aluminum-silicate network. Fastly reacting OPC/SiO₂ blend forms rigid interfacial phases shortly after the start of the hydration reactions, so the newly formed iron-containing interfacial products that take larger volume than the original protective layer on the steel produce a stress at the rigid interfacial layer that cannot accommodate the changes. After longer testing times, these amorphous products with Fe-O-Si linkage destroy the casing protective layer completely, detach cement sheath and spall, scale off the surface of the casing as rust leaving it unprotected from corrosion (Figure 15).

Along with the carbonation of the interface these scale-forming products destroy the cement-metal bond. The chemistry of the cement matrix does not have any capability to recover this bonding.

In the case of TSRC, the bond is partially destroyed with the formation of calcium carbonate. After 20 severe TS cycles cement has capacity to recover the bond, at least partially, through slow pozzolanic reactions of non-reacted FAF particles remaining in the cement.

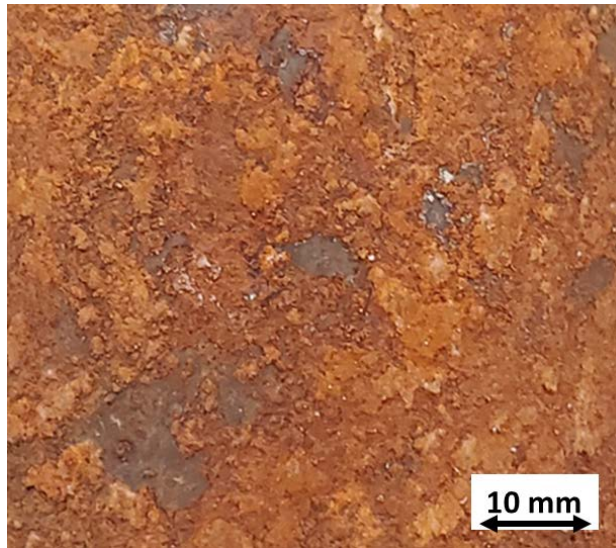


Figure 15: CS casing surface rust with Fe-O-Si linkages after 20 severe TS cycles of casing-OPC/SiO₂ cement sheath sample.

4. Conclusions

The following conclusions can be drawn from the presented results:

1. The common high-temperature well cement formulation cannot be used to provide the long-term integrity of high-temperature underground storage wells. The interfacial cement-metal bond fails first, followed by casing corrosion and failure. Twenty severe TS cycles clearly demonstrated that OPC-based composites cannot withstand severe TS conditions (one cycle: 250°C hydrothermal → dry 250°C → 18°C water through casing).

In the conducted tests the cement sheath broke in the first cycle forming wide continuous cracks, losing 84% of the bond strength and compromising CS corrosion protection so that severe corrosion of CS was observed already after a short testing time for samples cured in water. It is reasonable to assume that geothermal brines will further accelerate corrosion.

2. Advanced TSRC performed significantly better under the conditions of the severe stress: it lost 11% of its bond strength in 20 cycles (vs. 84% for Portland cement blend) and for the most part provided continuous protection of the casing from corrosion. However, TSRC formed thin non-continuous cracks that resulted in some CS corrosion after 20 severe TS cycles.
3. One of the possible reasons for the better TSRC bond durability was its slightly expansive behavior during the cycling.
4. The CTE changes in severe TS cycles were similar for both TSRC and OPC and unlike reported by other authors (Bu, Chang, Du, & Liu, 2017) could not account for the changes in mechanical properties of the interfacial bond, cement sheath damage and CS corrosion under the test conditions.
5. Phase change analyses demonstrated preferential formation of aluminum-rich phases at the interface and growing crystallinity of TSRC samples, accompanied by the decrease in the bond strength suggesting importance of amorphous aluminum-rich phases for the strong interfacial bond. This was confirmed by the moderate TS cement cycling. In the case of OPC/SiO₂ blend, amorphous phase with Fe-O-Si linkages was unfavorable for the bond durability, flaking off the casing as rust powder
6. Curing regime, in particular, rate of the temperature increase may significantly affect the bond strength. Cement shrinkage resulting in decreased bond-strength becomes an important factor when the heating rate is high. Leaving a storage well to slowly increase in temperature after the completion before injecting hot fluids may help to preserve metal-cement bonding.
7. Thirty moderate hydrothermal TS cycles (100 °C → 18 °C) did not compromise mechanical properties of the TSRC sheath on CS, both matrix compressive strength and interfacial bond strength increased during 30 cycles of thermal shock. The crystallization of cement was slow at this temperature and mostly amorphous hydrates and reaction products formed both in the matrix and at the interface providing strong durable bond. This fact suggests that the amorphous phase is favorable for the durable composite-metal bond and casing corrosion protection.
8. However, one concern was the continuous decrease in cement CTE during the moderate thermal cycling resulting in increasing difference between the cement and CS CTE and higher probability of the interfacial bond damage after repeated cycling.
9. FAF particles reacted only partially during the 30 moderate TS cycles and 20 severe TS cycles suggesting remaining self-healing capacity of the cement at longer curing times in case of a damage.
10. Performance of the tested composites might differ significantly if alloys are used instead of CS.
11. The future efforts to achieve durable interfacial bond should focus on increased cement flexibility and toughness to accommodate thermal stresses; this could be done by using foam cement and additives modifying the nature of the hydrates at the interface or both. The use of lightweight cement (foam or microspheres-modified) would bring another

benefit of well insulation minimizing heat losses in electric-generating operations. Control of rheological parameters with slurry modifiers (organic at lower temperatures and inorganic for higher temperatures) may help to form amorphous, dense interfacial layer, beneficial for durable bond. Cements with re-adhering ability of de-bonded sheath may further extend the life of storage geothermal wells.

Acknowledgement

This publication was based on the work supported by the Geothermal Technologies Office in the US Department of Energy (DOE) Office of Energy Efficiency and Renewable Energy (EERE) (project manager Arlene Anderson), under the auspices of the US DOE, Washington, DC, under contract No. DE-AC02-98CH 10886. Research was carried out in part at the Center for Functional Nanomaterials, Brookhaven National Laboratory, which is supported by the US Department of Energy, Office of Basic Energy Sciences, under Contract No. DE-SC0012704.

REFERENCES

- Berra, M., Fabbri, F., Facoetti, M., Noris, A., Pezzuoli, M., Ricciardulli, R., Tarquini, B. (1988). Behaviour of a cementing hydraulic binder under severe geothermal conditions. *Geothermics*, 17(5–6), 785–813. [https://doi.org/10.1016/0375-6505\(88\)90038-7](https://doi.org/10.1016/0375-6505(88)90038-7)
- Bu, Y., Chang, Z., Du, J., & Liu, D. (2017). Experimental study on the thermal expansion property and mechanical performance of oil well cement with carbonaceous admixtures. *RSC Advances*, 7(46), 29240–29254. <https://doi.org/10.1039/c7ra03504g>
- James, S. P., Schmalzried, T. P., McGarry, F. J., & Harris, W. H. (1993). Extensive porosity at the cement–femoral prosthesis interface: A preliminary study. *Journal of Biomedical Materials Research*, 27(1), 71–78. <https://doi.org/10.1002/jbm.820270110>
- Latham, K., Williams, C. D., & Duke, C. V. A. (1996). The synthesis of iron cancrinite using tetrahedral iron species, 2449(Vi), 15–18.
- Pyatina, T., & Sugama, T. (2014). Toughness improvement of geothermal well cement at up to 300°C: Using carbon microfiber. *Journal of Composite Materials*, 4, 177–190.
- Pyatina, T., Sugama, T., & Zaliznyak, T. (2017). Durability of bond between high-temperature cement composites and carbon steel. In *Transactions - Geothermal Resources Council* (Vol. 41).
- Sugama, T., & Pyatina, T. (2019). Self-healing, re-adhering, and corrosion-mitigating inorganic cement composites for geothermal wells at 270-300degC. *BNL-2019-IR*.
- Sugama, T., & Pyatina, T. (2019). Self-Healing , Re-adhering , and Corrosion-Mitigating Inorganic Cement Composites for Geothermal Wells at 270-300C. *BNL-211405-2019-INRE*, (February).
- Teodoriu, C., & Falcone, G. (2009). Comparing completion design in hydrocarbon and geothermal wells: The need to evaluate the integrity of casing connections subject to thermal stresses. *Geothermics*, 38(2), 238–246. <https://doi.org/10.1016/j.geothermics.2008.11.006>

Teodoriu, C., Kosinowski, C., Amani, M., Schubert, J., & Shadravan, A. (2013). Wellbore integrity and cement failure at HPHT conditions. *International Journal of Engineering and Applied Sciences*, 2, 1–13.